Semiclassical theory of strong localization for quantum thermalization

Christine Khripkov[1*], Amichay Vardi[1*], Doron Cohen[2*]
[1] *Department of Chemistry, Ben-Gurion University of the Negev, Beer-Sheva 84105, Israel*
[2] *Department of Physics, Ben-Gurion University of the Negev, Beer-Sheva 84105, Israel*

Abstract

We introduce a semiclassical theory for strong localization that may arise in the context of many-body thermalization. As a minimal model for thermalization we consider a few-site Bose-Hubbard model consisting of two weakly interacting subsystems that can exchange particles. The occupation of a subsystem (x) satisfies in the classical treatment a Fokker-Planck equation with a diffusion coefficient $D(x)$. We demonstrate that it is possible to deduce from the classical description a quantum breaktime t^*, and hence the manifestations of a strong localization effect. For this purpose it is essential to take the geometry of the energy shell into account, and to make a distinction between different notions of phase-space exploration.

Introduction

Equilibration in isolated bipartite systems is a major theme in many-body statistical mechanics. Hamiltonian classical or quantum dynamics can emulate thermalization between weakly-coupled constituent subsystems, provided at least one of them is classically chaotic, resulting in an ergodic evolution. The classical thermalization is then described by a Fokker-Planck equation (FPE) [1, 2] depicting a diffusive redistribution between the accessible states, with an implied fluctuation-dissipation theorem.

While chaos can provide the required ergodicity in a classical thermalization process, the corresponding quantum mechanical thermalization scenario [3–10] is endangered by the emergence of quantum localization [11–17]. Much effort has been invested in the study of many-body localization of large disordered arrays [18–24], but the physics of localisation in such large systems remain ambiguous. Even the definitions are vague, and the role of semiclassical phase-space structures with regard to the determination of the mobility edge has not been addressed [25]. It is therefore essential to consider tractable minimal models for thermalization, in which the origins of localisation can be traced. Such models should include two weakly coupled subsystems, where the classical chaoticity requirement imposes a minimum of two degrees of freedom on at least one of them.

One type of a model that is experimentally viable [26, 27], is the few-site Bose-Hubbard system [28–31]. Since the N-boson system has a clear classical limit with $1/N$ serving as an effective Planck constant, it is ideal for exploring many-body localization effects in a controlled manner. The two-site Bose-Hubbard model, also known as the bosonic Josephson junction, is excluded due to the integrability of its classical phase-space. The three-site system features low-dimensional chaos [28, 29], but it is of a little interest for quantum localization studies, because the classical phase-space is divided into disjoint territories by Kolmogorov-Arnold-Moser (KAM) tori. The nature of localization in the three-site system is therefore always semiclassical: due to trapping either on a quasi-integrable island, or inside a chaotic pond [29]. We therefore conclude that the smallest bi-partite Bose-Hubbard model which may demonstrate a quantum localization effect in its thermalization, is a four-site system [2] where the pertinent weakly-coupled subsystems are a chaotic trimer and a single auxiliary site denoted here as a 'monomer', see Fig. 1a.

Preliminary numerical evidence for localization in the dynamics of the four-site model has been obtained in [2]. In some phase-space regions localization is semiclassical: it originates from quasi-integrability and therefore persists in the classical limit. However, there are other phase-space regions that are classically completely chaotic, yet exhibit localization quantum mechanically. This Anderson-type localization does not survive in the classical limit.

Surprisingly, no semiclassical theory for strong localization in such a minimal model is currently available. The original view of Anderson [11] holds that strong localization appears due to interference of trajectories. This leads to the Anderson criterion which involves the *connectivity* of space. In certain cases it is possible to carry out a semiclassical summation, to identify families of destructively interfering trajectories, see, for example, Ref. [17]. However, this approach is a dead-end as far as physical insight is concerned. A different paradigm, namely, the scaling theory of localization [12], illuminates the importance of *dimensionality*. But, clearly, such an approach is designed for scalable disordered systems, and not for our model of interest which contains finite subsystems with few freedoms, and where idealized chaos of the random-matrix-theory-type cannot be assumed. We would like to have a theory that will deduce quantum localization from semiclassical simulations, without having to take the details of interference into account.

In this paper we argue that such a theory can be attained by an extension of a neglected paradigm [32–35] that regards quantum localization as the breakdown of quantum-classical correspondence (QCC). The idea is to

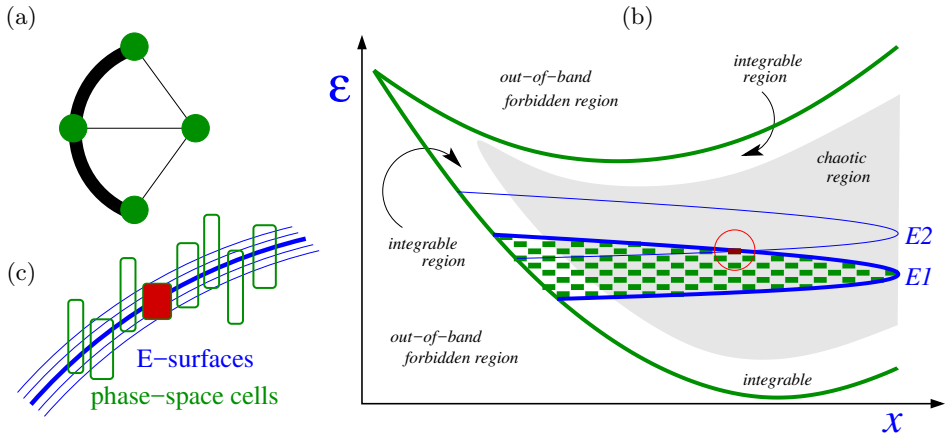

FIG. 1. **Illustration of the system and its phase-space.** **(a)** We consider $N = 60$ bosons in a four-site system that is formed by weakly coupling a trimer and a monomer subsystems. The trimer consists of three strongly coupled sites. The system is described by the Hamiltonian equation (9), see Methods. **(b)** The phase-space of the system is divided into cells that are labeled by $r = (x, \varepsilon)$. A given cell r_0 (circled and colored in red) overlaps with energy surfaces $E_1 < E < E_2$, forming a region that we call its "energy shell" (strictly speaking, we display the *projection* of a high-dimensional energy shell onto the two-dimensional plane). Each surface E overlaps with many cells, as shown schematically for E_1 (the white spaces between the cells are for visual purposes only). Note that the width in ε of the energy surface shrinks to zero as $x \to N$, where the trimer-monomer coupling term equation (10) vanishes. A single classical trajectory explores a zero-thickness energy surface E, and can visit at most Ω_E cells. To be precise, only a fraction $\mathcal{F}^{\rm cl}$ is explored, because Ω_E counts not only cells that belong to the chaotic sea, but also cells that reside in quasi-integrable regions. A semiclassical cloud that starts at r_0 explores a larger volume that includes all the accessible cells within the (thick) energy shell. **(c)** An abstract illustration of the high-dimensional energy surfaces. Each surface is associated with a quantum eigenstate E_α. The number of surfaces $\mathcal{N}_E$ that participate in the dynamics (overlaping with the red cell) might be much smaller than the number of cells Ω_E that intersect a given energy surface.

figure out a procedure that allows for the semiclassical determination of a quantum breaktime. Such an approach has been discussed in the past with regard to localization in Anderson-type models in $d = 1, 2, 3$ dimensions [34, 35], but its adaptation for the analysis of localization in complex systems has not been explored. Here, we construct the necessary semiclassical framework for a detailed study of strong quantum localization and present the necessary tools for its analysis. We are inspired by the work of Heller regarding phase-space exploration [36, 37] that has been used in the past mainly in the context of weak localization, a.k.a. scar theory [38, 39]. We use the four-site Bose-Hubbard model to benchmark this theory and demonstrate its feasibility.

Let us first construct a naive theory. Let x be a coordinate that describes the thermalization process. In our four-site minimal model it is the occupation of the trimer subsystem, with the monomer subsystem containing the remaining $N - x$ particles. We assume that in the classical description the system is chaotic within the relevant energy range, and accordingly, we can derive an FPE for the evolving probability distribution $p(x; t)$, as explained in [1]. This FPE requires the calculation of a diffusion coefficient $D(x)$. Inspired by the literature on Anderson localization in quasi-one-dimensional arrays [32–35] we might deduce an emergent localization length $\xi = g(x)D(x)$, where $g(x)$ is the density of states (given x) at the region of interest. It turns out that such an approach does not work. In fact, it should be obvious in advance that it cannot be a generally valid procedure, because the actual dimensionality of the system is completely ignored. Were it valid, it would have implied that any diffusing coordinate is doomed to be localized in the quantum treatment, irrespective of the existence of extra coordinates.

We therefore have to trace back one step, and to recall the argument that leads to the semiclassical expression for ξ. The idea is to generalize the QCC condition $t < t_H(\Omega)$, where Ω indicates the volume of the system, and $t_H = 2\pi/\Delta_0$ is the Heisenberg time, determined by the mean level spacing Δ_0. This generalization is performed by replacing the total Ω by the classically *explored* volume $\Omega_t^{\rm cl}$, such that the *running* Heisenberg time is now related to the *effective* level spacing; hence, the QCC condition becomes $t < t_H(\Omega_t)$. The breakdown of this condition [32–35] determines the breaktime t^*, and hence the localization volume.

The above is roughly the approach that we are going to employ. The challenge is to provide a proper phase-space formulation of the QCC condition, taking the non-trivial geometry of the energy shell into account. It is important to realize that the classical *exploration* volume, contrary to the intuitive thinking, is not the same volume over which the probability distribution $p(x; t)$ spreads after time t, henceforth named the *spreading* volume.

Results

Outline.– We define a quantum localization measure $\mathcal{F}^{\rm s}$ and demonstrate the manifestation of strong localization in our model system. The objective is to provide a semiclassical theory for the breaktime. This goal is attained in two stages: (a) The first step is to introduce definitions for the classical phase-space exploration function $\Omega_t^{\rm cl}$, and for the quantum Hilbert-space exploration function $\mathcal{N}_t^{\rm qm}$. Associated with it is the distinction between Ω_E that counts the cells that intersect a given energy surface, and $\mathcal{N}_E$ that measures the width of the energy shell. This leads naturally to the definition of the classical and the quantum ergodicity measures $\mathcal{F}^{\rm cl}$ and $\mathcal{F}^{\rm qm}$; (b) The second step is to formulate a phase-space version for the QCC condition:

$$\mathcal{N}_t^{\rm sc} \quad < \quad \mathcal{F}_{\rm erg}^{\rm qm}\left[\frac{\mathcal{N}_E}{\Omega_E}\right]\Omega_t^{\rm cl} \tag{1}$$

Here $\mathcal{N}_t^{\rm sc} \approx t/t_E$ is the semiclassical estimate for the quantum exploration, which depends crucially on a time scale t_E, determined by the width of the energy shell. The quantum factor $\mathcal{F}_{\rm erg}^{\rm qm} = 1/3$ is required to account for universal quantum fluctuations.

We then demonstrate that the above phase-space version of the QCC condition provides a reliable and accurate estimate for the breaktime and for the localization volume in our minimal model for many-body thermalization. Additional technical details are provided in the Methods section, and in the Supplementary.

Dynamical localization measure

Consider a system whose state-space is spanned by a *discrete* basis of 'locations' $|r\rangle$. In the quantum context these locations are eigenstates of some unperturbed Hamiltonian $\mathcal{H}_0$, while in the classical context they are *Planck cells* of volume h^d, where d is the number of freedoms, and h is the Planck constant. A sketch of the phase-space for our model system is displayed in Fig. 1b,c. The cells are labeled by $r = (x, \varepsilon)$, where x is the occupation of the trimer and ε is the unperturbed energy in the absence of coupling between the constituent subsystems.

The dynamics is generated by a different Hamiltonian $\mathcal{H}$, either semi-classically ("sc") or quantum-mechanically ("qm"). The perturbation is the coupling of the two subsystems. The system is launched at $|r_0\rangle$. In the quantum case this state is propagated using the unitary evolution operator. The corresponding semiclassical simulation refers to a cloud of classical trajectories initiated within the cell r_0 and propagated using the classical equations of motion. If the motion is classically chaotic, we typically observe a stochastic-like evolution. It is important to emphasize that $\hbar$ is implicit in the semiclassical context via the definition of the "volume" of a Planck cell, but otherwise it has no effect on the classical dynamics.

After time t the state of the system is characterized by a probability distribution $P_t(r|r_0)$. Such distributions are illustrated in Fig. 2a,b, and projected onto x in Fig. 2c. The plotted distributions clearly show that if the model system is launched in a state with high trimer population, it remains quantum mechanically localized despite its classical ergodization.

For each initial state r_0, one can define a spreading volume Ω_t that counts how many r-locations participate in the $P_t(r|r_0)$ distribution. Optionally, one can define for the same initial preparation the spreading volume L_t in x. Results for the saturation value L_∞ as a function of the initial value of x are displayed in Fig. 2d.

We define a dynamical localization measure as the fraction of the semiclassical spreading volume covered by the quantum evolution, i.e.

$$\mathcal{F}^{\rm s} \quad \equiv \quad \frac{\Omega_\infty^{\rm qm}}{\Omega_\infty^{\rm sc}} \tag{2}$$

Strong dynamical localization means that the quantum distributions occupies a small fraction of the classical spreading volume and hence $\mathcal{F}^{\rm s} \ll 1$. In the Anderson model of localization, $\Omega_\infty^{\rm sc}$ corresponds to the total volume L^d of a d-dimensional disordered lattice, while $\Omega_\infty^{\rm qm}$ corresponds to some localization volume ξ^d. The term "dynamical localization" has been introduced in the quantum chaos literature in connection with the standard map, a.k.a. the "kicked rotor", where the explored "locations" are angular momentum states [13–16]. By now it is recognized that both *disorder* or *chaos* can lead to strong localization effect.

Space exploration

The notion of *exploration*, as opposed to *spreading*, is a key concept in the formulation below. We treat this notion on equal footing for both the classical and for the quantum cases. The classical definition of "phase-space exploration" is inspired by old works on random walk on a lattice [40], while the quantum notion of "Hilbert-space exploration" is adopted from [36]. The evolving state of a system is described by a delta-distribution (a point) in phase-space in the classical case ("cl"), or by a cloud of points in the semiclassical case ("sc"), or by a probability matrix in the quantum ("qm") case. Either way, we use the notations $\varrho(t)$ for the instantaneous state of the system, and $\overline{\varrho}(t)$ for its average during the time interval $[0, t]$, namely,

$$\overline{\varrho}(t) \quad \equiv \quad \frac{1}{t}\int_0^t \varrho(t')dt' \ . \tag{3}$$

The explored space is then defined as,

$$\left\{\begin{matrix}\Omega_t^{\rm cl}\\ \mathcal{N}_t^{\rm qm}\end{matrix}\right\} \quad \equiv \quad \left\{\text{trace}\left[\overline{\varrho}(t)^2\right]\right\}^{-1} \tag{4}$$

These functions tell us what is the minimal number of cells or basis-states that are required in order to describe

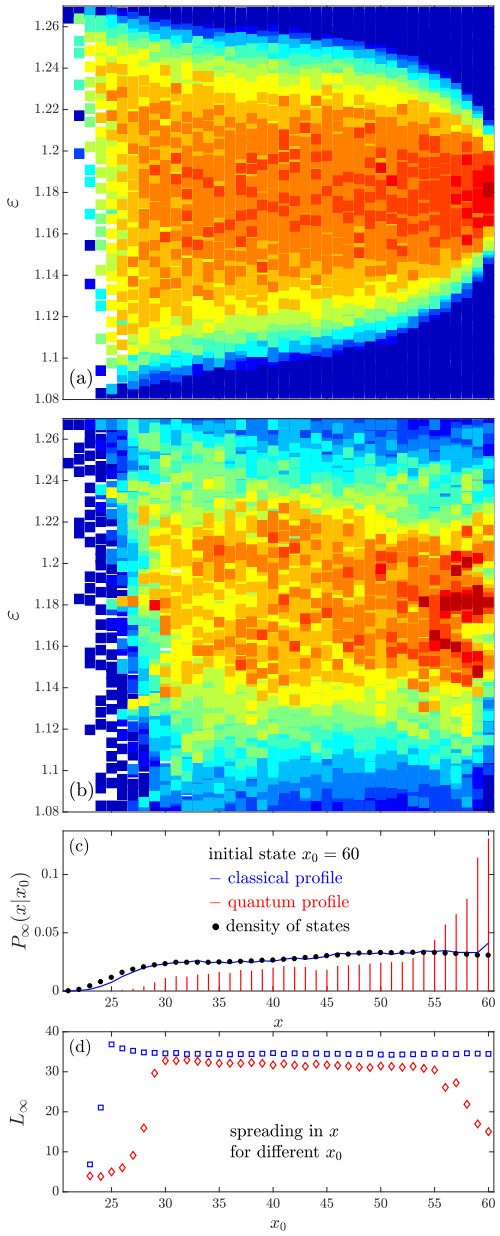

FIG. 2. **The quantum localization effect.** Panels (a) and (b) display the two-dimensional saturation profile $P_\infty(r|r_0)$ for the semiclassical and the quantum simulations, respectively. The initial condition r_0 corresponds to having all particles in the trimer ($x_0 = 60$) with an energy $\varepsilon = 1.181$. The color scale encodes the probability from low (blue) to high (red). The semiclassical simulation in (a) provides the determination of the energy shell. The quantum simulation exhibits strong localization. In panel (c) the distribution is projected onto x space. The quantum (red) simulation features a peak at the initial x_0, unlike the semiclassical (blue) simulation that reflects phase-space ergodicity, as implied by the great agreement with the (black) density of states $g(x)$. Panel (d) displays the spreading length L_∞ for different values of x_0. The low values of the semiclassical spreading (blue symbols) for $x_0 = 23$ and $x_0 = 24$ indicate a lack of classical ergodicity, and hence are of no interest for us. Our objective is to provide a theory for the *quantum* spreading (red symbols), where strong localization shows up in the range $24 < x_0 < 30$ and for $x_0 > 55$.

the time-dependent dynamics up to time t. The classical function $\Omega_t^{\rm cl}$ counts how many cells have been visited by the trajectory, while the quantum function $\mathcal{N}_t^{\rm qm}$ counts the number of states that participate in the dynamics during this time. The latter is related to the survival probability, see equation (17) of the Methods. From this relation (see there) it follows that the short time dynamics can be semiclassically approximated by $\mathcal{N}_t^{\rm sc} \approx t/t_E$, where $t_E = 2\pi/\Delta_E$ reflects the width of the energy shell. On the other extreme, for long times $\mathcal{N}_t^{\rm qm}$ approaches a limiting value $\mathcal{N}_\infty$ that counts the total number of eigenstates that participate in the time evolution.

It is now possible to define classical and quantum measures for ergodicity. The classical measure is

$$\mathcal{F}^{\rm cl} \equiv \frac{\Omega_\infty^{\rm cl}}{\Omega_E} \tag{5}$$

where Ω_E is the total number of cells within the energy shell. We get $\mathcal{F}^{\rm cl} = 1$ only if the energy shell is fully chaotic without any quasi-integrable islands. The quantum ergodicity measure that has been proposed by [36] is defined in an analogous way:

$$\mathcal{F}^{\rm qm} \equiv \frac{\mathcal{N}_\infty}{\mathcal{N}_E} \tag{6}$$

where $\mathcal{N}_E$ is the number of states within the energy shell, see Methods for its precise definition. For quantum-ergodic dynamics of the GOE type one expects $\mathcal{F}_{\rm erg}^{\rm qm} = 1/3$. This well-known value reflects the universal effect of quantum fluctuations, and the statistical nature of the quantum-ergodic distribution.

It should be clear from the illustration in Fig. 1c that in general $\mathcal{N}_E$ can be much smaller than Ω_E. In fact, $\mathcal{N}_E$ is the volume of the local density of states (LDOS). The quantum LDOS density $\rho(E)$ (see Methods for its precise definition) provides the weight of the perturbed eigenstates E_α in the superposition that forms the initial state r_0. Similarly, the classical LDOS is the overlap of the initial Planck cell with various energy surfaces of the perturbed system. Fig. 3 displays the quantum and classical LDOS for representative preparations. Dynamical localization is implied when the quantum LDOS does not fill the classical LDOS envelope. This can be simply due to it being narrower than the classical width (localization in E) or due to its 'sparsity' within the classical envelope (localization in x). Fig. 4a displays the entire spectrum of the unperturbed states $|r_0\rangle$. For each r_0 the LDOS is calculated, and $\mathcal{F}^{\rm qm}$ is extracted. The red-coded states are quantum-ergodic, while the blue-coded states reside in region where the eigenstates are localized. This is confirmed by Fig. 4a where the eigenstates $|E_\alpha\rangle$ are color-coded according to their $\mathrm{var}(x)_\alpha$.

It is important not to confuse the explored volume with the *spreading* volume. The functions $\Omega_t^{\rm sc}$ and $\Omega_t^{\rm qm}$ count how many r cells or states are occupied by the evolving

distribution $P_t(r|r_0)$. The expected saturation value is

$$\Omega_\infty^{\rm sc} \approx \sqrt{\mathcal{N}_E^2+\Omega_E^2} \quad (7)$$

where $\mathcal{N}_E$, unlike Ω_E, is r_0-dependent. If the energy shell has a trivial "flat" geometry, such that $\mathcal{N}_E$ unperturbed states mix into $\mathcal{N}_E$ perturbed states in the same energy range Δ_E, then it follows that $\mathcal{N}_E=\Omega_E$, and hence $\Omega_\infty^{\rm sc}\approx\sqrt{2}\Omega_E$.

In Fig. 5 the explored and the spreading volumes are plotted as a function of time for a representative initial condition. The classical exploration that is described by $\Omega_t^{\rm cl}$ is much slower compared to the semiclassical spreading $\Omega_t^{\rm sc}$. In fact, it does not even saturate during the time interval that is displayed in the figure (though it does reach the saturation value that is indicated in the figure, but only after a much longer time). Irrespective of that, we establish in Fig. 6a that the system is classically ergodic for any $x_0>25$. We note that the boundary of the chaotic region in Fig. 1b has been determined numerically in [2] using a different method.

The slowness of the classical exploration constitutes an indication for the high-dimensionality of phase-space, and plays a major role in the determination of the breaktime. The quantum exploration and spreading volumes $\Omega_t^{\rm qm}$ and $\mathcal{N}_t^{\rm qm}$ are also displayed in Fig. 5. In a sense, our objective is to extract their time dependence from the classical time dependence.

QCC, breaktime and localization

Our purpose is to deduce localization from QCC considerations. For classical diffusive system the running Heisenberg time is determined by the number of sites that are explored during a random walk process. In the present context $\Omega_t^{\rm cl}$ counts cells in phase-space that are visited by a chaotic trajectory. The standard Heisenberg time $t_H=2\pi/\Delta_0$ is calculated for the total volume, hence the running Heisenberg time is $t_H(\Omega_t^{\rm cl})=[\Omega_t^{\rm cl}/\Omega_E]t_H$. The time scale that is associated with the width of the energy shell is $t_E=2\pi/\Delta_E$, and for the ratio we get $t_H/t_E=\mathcal{N}_E$, see Methods. It follows that the QCC condition $t<t_H(\Omega_t^{\rm cl})$ can be written as $(t/t_E)<(\mathcal{N}_E/\Omega_E)\Omega_t^{\rm cl}$. We identify the left hand side as the semiclassical approximation for the Hilbert-space exploration. We also know that for a quantum-ergodic system in a "flat", fully chaotic energy shell, the saturation is attained once $\mathcal{N}_t^{\rm qm}\approx\mathcal{F}_{\rm erg}^{\rm qm}\mathcal{N}_E$, with $\mathcal{F}_{\rm erg}^{\rm qm}=1/3$ for GOE statistics. We therefore conjecture that the general QCC condition is equation (1) without any undetermined prefactors.

The numerical determination of the breaktime t^* for our model system is demonstrated in Fig. 5 for a representative initial condition. The results for other values of x_0 are presented in Fig. 6b. The quantum saturation volume is estimates as follows:

$$\Omega_\infty^{\rm qm}\Big|_{\rm predicted} = \mathcal{F}_{\rm erg}^{\rm s}\,\Omega_{t*}^{\rm sc} \quad (8)$$

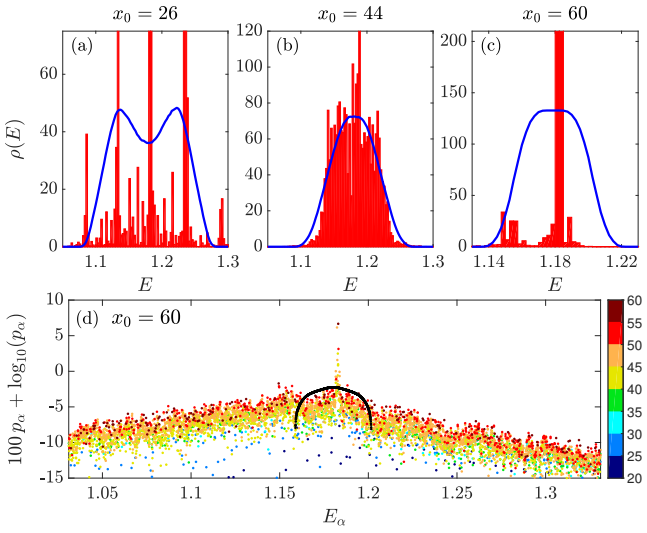

FIG. 3. **Signatures of localization in the LDOS.** Panels (a,b,c) compare the quantum LDOS (red) with its semiclassical counterpart (blue). In the quantum case, the density $\rho(E)$ is smoothed over an energy scale that corresponds to 50 level spacing. Quantum ergodicity is reflected in panel (b) where the LDOS matches well the semiclassical envelope. Quantum localization is reflected in panels (a) and (c). The vertical axis has been zoomed in (a,c) and hence the peaks are chopped. Note also the reduced range of the horizontal axis in panel (c). Panel (d) provides a sharper view of panel (c). It displays the bare probabilities p_α instead of the smoothed density $\rho(E)$, and uses a non-linear scale (vertical axis) to resolve both high and low values. The quantum symbols are color-coded according to the value of $\langle x\rangle_\alpha$. The semiclassical LDOS is the black line. We observe that localization is present both in E and in x. The localization in x is reflected as sparsity: there are many low lying blue points that correspond to small $\langle x\rangle_\alpha$ values, and few high-lying red points that correspond to large values.

The ergodic value $\mathcal{F}_{\rm erg}^{\rm s}\approx 2/3$ is used as a calibration factor. Thus, using equation (8) we obtain a prediction for the localization measure $\mathcal{F}^{\rm s}$ for any other value of x_0. The results are summarized in Fig. 6c, and the agreement with the quantum simulation is outstanding. For sake of comparison, we also display the results for the quantum ergodicity measure $\mathcal{F}^{\rm qm}$.

For completeness, we would like to reconstruct the results for the breaktime in the case of a homogeneous diffusive system in d dimensions. In one dimension, $\Omega_t^{\rm cl}\approx\sqrt{D_0 t}$ and therefore there is always a breaktime at $t^*=t_E^2 D_0$, which implies the well-known proportionality between the diffusion coefficient and the localization length. In $d>2$ dimensions the explored volume depends linearly on the time, $\Omega_t^{\rm cl}\approx c_0+v_0 t$, which implies a mobility edge. Namely, a breaktime exists, and hence localization is observed, if $\mathrm{g}<\mathrm{g}_c$, where $\mathrm{g}\equiv v_0 t_E$ and $\mathrm{g}_c=1$. In the type of system that we have studied the phase-space dynamics is complicated, and a simple diffusion law does not apply. Still, by using the QCC condition

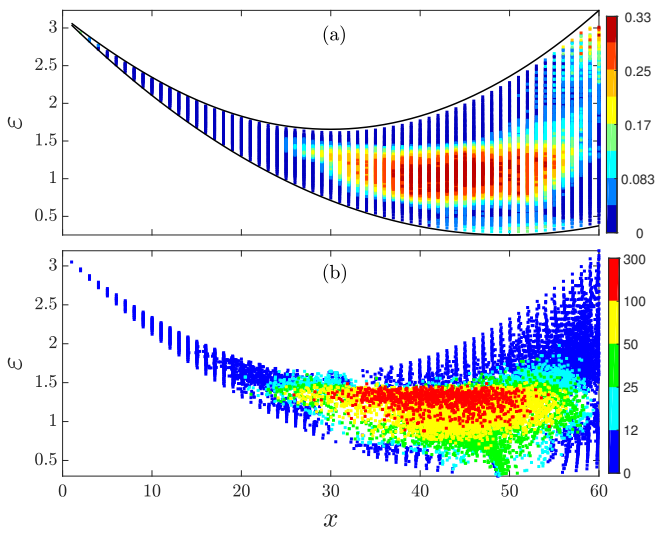

FIG. 4. **The quantum spectrum.** **(a)** The unperturbed states $|r\rangle = |x, \varepsilon\rangle$ are color-coded according to $\mathcal{F}^{\rm qm}$. Red color implies quantum ergodicity as in the LDOS of Fig.3b. By contrast, states with low $\mathcal{F}^{\rm qm}$ (blue) exhibit strong quantum localization. **(b)** The perturbed states $|E_\alpha\rangle$ are color-coded according to $\mathrm{var}(x)_\alpha$, and positioned according to $(\langle x\rangle_\alpha, \langle \varepsilon\rangle_\alpha)$. The low-variance states (blue) have significant overlaps only with unperturbed states for which $x \approx \langle x\rangle_\alpha$, while the large-variance states (red) correspond to microcanonical states within the chaotic sea.

equation (1) we are able to deduce whether dynamical localization shows up, and also to provide a very good quantitative estimate for the localization measure.

Discussion

Most of the literature about strong localization, including "quantum chaos" studies of periodically driven systems (e.g. the Kicked Rotor), concerns Anderson-like scalable models where the energy shell is "flat", such that transfer-matrix or scaling theory related methods apply. In contrast, in the present work we have treated a complex system that possesses a complicated phase-space, where semiclassical localization in quasi-integrable islands, as well as Anderson-type localization in some regions of the chaotic sea, manifest themselves.

The trimer-monomer configuration that we have considered can be regarded as the building block for the study of many-body thermalization in large arrays, as discussed by [8]. We were able to determine the quantum breaktime based on purely classical simulations. Furthermore, our procedure has provided predictions that were in a remarkable agreement with the quantum localization measures.

The proposed semiclassical procedure is relevant not only for the thermalization problem. In recent works [29, 30] it has been demonstrated that the stability of the super-flow in a three-site Bose-Hubbard ring is de-

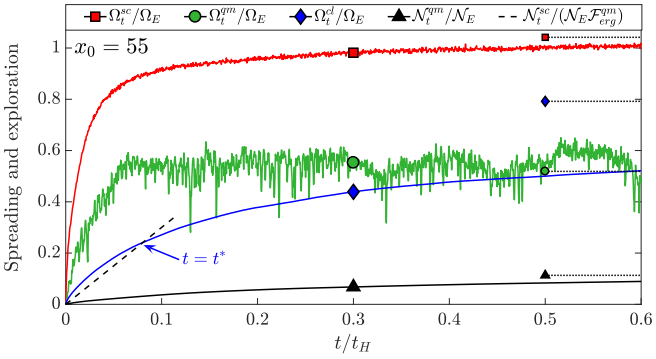

FIG. 5. **Breaktime determination.** The functions $\Omega_t^{\rm cl}$, $\Omega_t^{\rm sc}$, $\Omega_t^{\rm qm}$, and $\mathcal{N}_t^{\rm qm}$ are plotted versus time (see legend). Each simulation starts with $x_0 = 55$ particles on the trimer. The saturation values are indicated by dotted horizontal lines. The semiclassical estimate for the breaktime, based on equation (1), is determined by the intersection of the dashed line with $\Omega_t^{\rm cl}$.

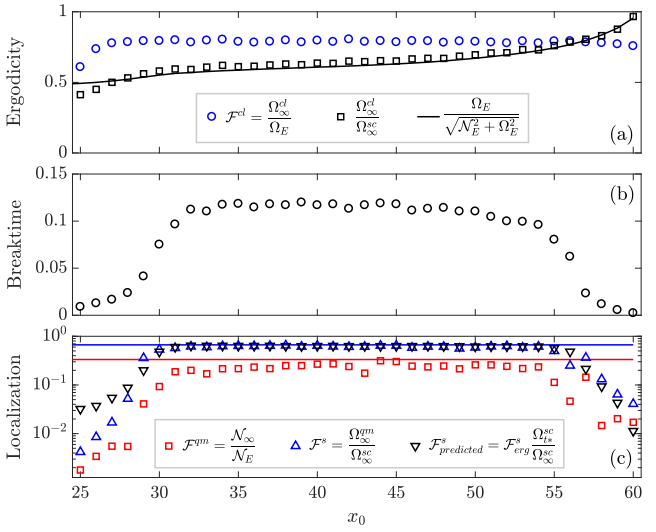

FIG. 6. **Semiclassical prediction of strong localization.** **(a)** Our interest is focused in the range of x_0 where $\mathcal{F}^{\rm cl}$ indicates a nearly ergodic classical motion. Note that 100% ergodicity cannot be reached because each energy surface contains inaccessible quasi-regular regions. A secondary test for ergodicity is the agreement between the exploration-spreading ratio (squares) and it ergodic value (line) which is implied by equation (7). **(b)** The scaled breaktime t^*/t_H is deduced from equation (1) via the procedure that has been illustrated in Fig. 5. **(c)** The quantum ergodization measure $\mathcal{F}^{\rm qm}$ and the dynamical localization measure $\mathcal{F}^{\rm s}$ for different initial conditions. The horizontal red and blue lines mark the ergodic values $\mathcal{F}^{\rm qm}_{\rm erg} = 1/3$ and $\mathcal{F}^{\rm s}_{\rm erg} = 2/3$, respectively, that are attained for simulations with $30 < x_0 < 55$. The prediction for $\mathcal{F}^{\rm s}$ is based on the semiclassical breaktime estimate. Note that an outstanding agreement persists for values as small as $\mathcal{F} \sim 10^{-2}$. The deviation at small x_0 is apparently related to remnants of quasi-integrability.

termined either by the Landau-criterion, or by KAM dynamical stability. But for circuits with more than three sites, the KAM tori are not effective for the stabilization of the super-flow due to Arnold diffusion (see Supplementary). Thus the existence of dynamically-stable superfluidity in such circuits has to do with dynamical localization. The theoretical approach that we have presented allows, in principle, the determination of the superfluidity regime diagram for such devices where the high-dimensional chaos exhibits a slow exploration rate in the classical (large N) limit.

Methods

The model

The trimer-monomer of Fig. 1a is described by the Bose-Hubbard Hamiltonian $\mathcal{H} = \mathcal{H}_0 + \mathcal{H}_c$, where

$$\mathcal{H} \;=\; \frac{U}{2}\sum_{j=0}^{3}\hat{n}_j^2 - \frac{K}{2}(\hat{a}_1^\dagger\hat{a}_2 + \hat{a}_1^\dagger\hat{a}_3 + \text{h.c.}) + \mathcal{H}_c \quad (9)$$

and the trimer-monomer coupling term is

$$\mathcal{H}_c \;=\; -\frac{K_c}{2}\sum_{j=1}^{3}(\hat{a}_0^\dagger\hat{a}_j + \text{h.c.}) \quad (10)$$

The operators $\hat{a}_j^\dagger$, $\hat{a}_j$ and $\hat{n}_j = \hat{a}_j^\dagger\hat{a}_j$ create, destroy and count particles at site j. The parameter U is the on-site interaction, while K and $K_c \ll K, UN$ are the hopping frequencies ($\hbar = 1$). In the absence of coupling the Hamiltonian $\mathcal{H}_0$ conserves the total trimer population $\hat{x} \equiv \hat{n}_1 + \hat{n}_2 + \hat{n}_3$, hence x is a good quantum number for the unperturbed eigenstates. Another good quantum number is the scaled energy $\varepsilon = \langle\mathcal{H}_0\rangle/(NK)$, hence we use the notation $|r\rangle = |x, \varepsilon\rangle$. Similarly scaled perturbed eigenenergies are $E_\alpha = \langle\mathcal{H}\rangle/(NK)$. The classical limit is obtained by replacing the bosonic operators with c numbers, namely $\hat{a}_j \to \sqrt{n_j}\exp(i\varphi_j)$. Standard rescaling implies that the dimensionless classical parameters are $u = NU/K$ and $k = K_c/K$, while the effective Planck constant is $1/N$. In the simulations we set $u = 6.3$ and $k = 0.1$, and the time units are chosen such that $K = 1$.

Basic definitions

The overlaps between the eigenstates $|r\rangle$ of $\mathcal{H}_0$ and the eigenstates $|E_\alpha\rangle$ of $\mathcal{H}$ form a probability kernel

$$\rho(r|E_\alpha) \;=\; |\langle r|E_\alpha\rangle|^2 \quad (11)$$

Within the semiclassical framework, this kernel is calculated via a phase-space integral over the product of Liouville distributions that represent the Planck-cell r and the microcanonical shell E_α. For a given r_0 we define the notation $p_\alpha = \rho(r_0|E_\alpha)$. The local density of states (LDOS) is the associated distribution

$$\rho(E) \;=\; \sum_\alpha p_\alpha\; 2\pi\delta(E - E_\alpha) \quad (12)$$

It is normalized with respect to the measure $dE/(2\pi)$. The semiclassical LDOS, denoted $\rho^{\text{sc}}(E)$, is the distribution of energies of the points within a Planck cell. The classical width of the energy shell is

$$\Delta_E \;=\; 2\pi\left\{\int_{-\infty}^{\infty}\left[\rho^{\text{sc}}(E)\right]^2\frac{dE}{2\pi}\right\}^{-1} \;\equiv\; \frac{2\pi}{t_E} \quad (13)$$

The total number of energy eigenstates that participate in the evolution of the state $|r_0\rangle$ is

$$\mathcal{N}_\infty \;=\; \left[\sum_\alpha p_\alpha^2\right]^{-1} \quad (14)$$

The total number of energy eigenstates within the energy shell is possibly larger. In order to determine this volume we set $p_\alpha^{\text{sc}} = [\Delta_0/(2\pi)]\rho^{\text{sc}}(E_\alpha)$ and get

$$\mathcal{N}_E \;=\; \frac{\Delta_E}{\Delta_0} \;=\; \frac{t_H}{t_E} \quad (15)$$

where the Heisenberg time is defined as $t_H = 2\pi/\Delta_0$. The measure for quantum ergodicity equation (6) is the fraction of eigenstates within the energy shell that "participate" in the dynamics.

The Fourier transform of the LDOS yields the survival probability:

$$\mathcal{P}(t) \;=\; \left|\int_{-\infty}^{\infty}\rho(E)\; e^{-iEt}\;\frac{dE}{2\pi}\right|^2 \quad (16)$$

The semiclassical approximation $\mathcal{P}^{\text{sc}}(t)$ is obtained via the Fourier transform of the semiclassical LDOS, and features an initial decay within the time t_E, which reflects the width of the classical envelope. The quantum $\mathcal{P}(t)$ departs after a longer time, and approaches $1/\mathcal{N}_\infty$, which reflects the number of participating eigenstates. The Hilbert-space exploration function is deduced from

$$\mathcal{N}_t^{\text{qm}} \;=\; \left[\frac{2}{t}\int_0^t\left(1 - \frac{\tau}{t}\right)\mathcal{P}(\tau)d\tau\right]^{-1} \quad (17)$$

This relation [36] follow from the definition equation (4) based on the observation that trace$[\varrho(t'+\tau)\varrho(t')]$ is invariant with respect to t', and hence equals $\mathcal{P}(\tau)$. An analogous relation does *not* hold in the semiclassical case, where $\varrho^{\text{sc}}(t)$ becomes irreversible due to the coarse-graining that is implied by the partitioning of the phase-space into cells. If we substituted $\varrho^{\text{sc}}(t)$ into equation (4), we would get Ω_t^{sc}, and *not* an approximation for the Hilbert space exploration function. However, we still

can obtain a semiclassical approximation $\mathcal{N}_t^{\rm sc}$ from equation (17) using $\mathcal{P}^{\rm sc}(t)$. After a transient, and disregarding recurrences, one obtains

$$\mathcal{N}_t^{\rm sc} \;\approx\; \left[\frac{2}{t}\int_0^t \mathcal{P}^{\rm sc}(\tau)d\tau\right]^{-1} \;=\; \frac{t}{t_E} \tag{18}$$

In the other extreme, for long times, the semiclassical approximation is not applicable, and $\mathcal{N}_t^{\rm qm}$ reaches the saturation value $\mathcal{N}_\infty$ of equation (14).

The phase-space spreading is described by the probability kernel $P_t(r|r_0)$. In the semiclassical case it is the fraction of the cloud that occupies the cell r at time t. In the quantum case it is $|\langle r|\,\exp(-i\mathcal{H}t)\,|r_0\rangle|^2$. The saturation profile can be obtained via convolution from the LDOS, namely

$$P_\infty^{\rm qm}(r|r_0) \;=\; \sum_\alpha \rho(r|E_\alpha)\,\rho(r_0|E_\alpha) \tag{19}$$

The phase-space spreading is evaluated as follows

$$\Omega_t^{\rm qm/sc} \;=\; \left\{\sum_r \Big[P_t(r|r_0)\Big]^2\right\}^{-1} \tag{20}$$

The semiclassical saturation value $\Omega_\infty^{\rm sc}$ measures the accessible volume of the energy shell. Projecting the distribution onto x space, one can define in the same manner the "spatial" spreading L_t, and its saturation value L_∞.

[1] I. Tikhonenkov, A. Vardi, J.R. Anglin, D. Cohen, *Minimal Fokker-Planck theory for the thermalization of mesoscopic subsystems*, Phys. Rev. Lett. **110**, 050401 (2013).

[2] C. Khripkov, A. Vardi, and D. Cohen, *Quantum thermalization: anomalous slow relaxation due to percolation-like dynamics*, New J. Phys. **17**, 023071 (2015).

[3] M. Srednicki, *Chaos and quantum thermalization*, Phys. Rev. E **50**, 888 (1994).

[4] M. Rigol, V. Dunjko, and M. Olshanii, *Thermalization and its mechanism for generic isolated quantum systems*, Nature **452**, 854 (2008).

[5] A. Polkovnikov, K. Sengupta, A. Silva, M. Vengalattore, *Colloquium: Nonequilibrium dynamics of closed interacting quantum systems*, Rev. Mod. Phys. **83**, 863 (2011).

[6] M. Gring, M. Kuhnert, T. Langen, T. Kitagawa, B. Rauer, M. Schreitl, I. Mazets, D. Adu Smith, E. Demler, J. Schmiedmayer, *Relaxation and Prethermalization in an Isolated Quantum System*, Science **337**, 1318 (2012)

[7] M. Olshanii, K. Jacobs, M. Rigol, V. Dunjko, H. Kennard, and V. A. Yurovsky, *An exactly solvable model for the integrability-chaos transition in rough quantum billiards*, Nature Communications **3**, 641 (2013).

[8] D. M. Basko, *Weak chaos in the disordered nonlinear Schrödinger chain: Destruction of Anderson localization by Arnold diffusion*, Ann. Phys. **326**, 1577 (2011).

[9] L. F. Santos, F. Borgonovi, and F. M. Izrailev, *Chaos and Statistical Relaxation in Quantum Systems of Interacting Particles*, Phys. Rev. Lett. **108**, 094102 (2012).

[10] F. Borgonovi, F.M. Izrailev, L.F. Santos, V.G. Zelevinsky, *Quantum chaos and thermalization in isolated systems of interacting particles*, Phys. Rep. **626**, 1 (2016).

[11] P. W. Anderson, *Absence of Diffusion in Certain Random Lattices*, Phys. Rev. **109**, 1492 (1958).

[12] E. Abrahams, P. W. Anderson, D. C. Licciardello, and T. V. Ramakrishnan, *Scaling Theory of Localization: Absence of Quantum Diffusion in Two Dimensions*, Phys. Rev. Lett. **42**, 673 (1979).

[13] G. Casati, B. V. Chirikov, F. M. Izrailev, and J. Ford, in *Stochastic Behaviour in classical and Quantum Hamiltonian Systems*, Vol. 93 of Lecture Notes in Physics, ed. by G. Casati and J. Ford (Springer, N. Y. 1979), p. 334.

[14] S. Fishman, D. R. Grempel, and R. E. Prange, *Chaos, Quantum Recurrences, and Anderson Localization*, Phys. Rev. Lett. **49**, 509 (1982).

[15] F. Haake, M. Kus, and R. Scharf, *Classical and Quantum Chaos for a Kicked Top*, Z. Phys. B **65**, 381 (1986).

[16] F. Haake, *Quantum Signatures of Chaos* (Springer, Berlin, 2001).

[17] H. Schanz, U. Smilansky, *Periodic-orbit theory of Anderson localization on graphs*, Phys. Rev. Lett. **84**, 1427 (2000).

[18] I.V. Gornyi, A.D. Mirlin, D.G. Polyakov, *Interacting electrons in disordered wires: Anderson localization and Low-T transport*, Phys. Rev. Lett. **95**, 206603 (2005).

[19] D. Basko, I. L. Aleiner, and B. Altshuler, *Metal-insulator transition in a weakly interacting many-electron system with localized single-particle states*, Ann. Phys. **321**, 1126 (2006).

[20] I.L. Aleiner, B.L. Altshuler, G.V. Shlyapnikov, *A finite-temperature phase transition for disordered weakly interacting bosons in one dimension*, Nature Physics **6**, 900 (2010).

[21] R. Berkovits, *Entanglement entropy in a one-dimensional disordered interacting system: the role of localization*, Phys. Rev. Lett. **108**, 176803 (2012).

[22] Y. Bar Lev and D. R. Reichman, *Dynamics of many-body localization*, Phys. Rev. B **89**, 220201(R) (2014).

[23] E. J. Torres-Herrera and L. F. Santos, *Dynamics at the many-body localization transition*, Phys. Rev. B **92**, 014208 (2015).

[24] M. Tavora, E. J. Torres-Herrera, L. F. Santos, *Power-law decay exponents: a dynamical criterion for predicting thermalization*, Phys. Rev. A **95**, 013604 (2017).

[25] D. J. Luitz, Y. Bar Lev, *The Ergodic Side of the Many-Body Localization Transition*, Ann. Phys. (Berlin) 1600350 (2017), and further reference therein.

[26] O. Morsch and M. Oberthaler, *Dynamics of Bose-Einstein condensates in optical lattices*, Rev. Mod. Phys. **78**, 179 (2006).

[27] I. Bloch, J. Dalibard, and W. Zwerger, *Many-body physics with ultracold gases*, Rev. Mod. Phys. **80**, 885 (2008).

[28] M. Hiller, T. Kottos, and T. Geisel, *Wave-packet dynamics in energy space of a chaotic trimeric Bose-Hubbard system*, Phys. Rev. A **79**, 023621 (2009), *and further references therein.*

[29] G. Arwas, A. Vardi, and D. Cohen, *Superfluidity and Chaos in low dimensional circuits*, Scientific Reports **5**, 13433 (2015).

[30] G. Arwas and D. Cohen, *Superfluidity in Bose-Hubbard circuits*, Phys. Rev. B **95**, 054505 (2017).

[31] H. Hennig and R. Fleischmann, *Nature of self-localization of Bose-Einstein condensates in optical lattices*, Phys. Rev. A **87**, 033605 (2013).

[32] B. V. Chirikov, F. M. Izrailev, D. L. Shepelyansky, *Dynamical stochasticity in classical and quantum mechanics*, Sov. Scient. Rev. C **2**, 209 (1981) [Section C—Mathematical Physics Reviews, ed. by S. P. Novikov, Vol. 2 (Harwood Academic Publishers, Chur 1981)]

[33] D. L. Shepelyansky *Localization of diffusive excitation in multi-level systems*, Physica D **28**, 103, (1987).

[34] T. Dittrich, *Spectral statistics for 1-D disordered systems: a semiclassical approach*, Phys. Rep. **271**, 267 (1996).

[35] D. Cohen, *Periodic orbits, breaktime and localization*, J. Phys. A **31**, 277 (1998).

[36] E. J. Heller, *Quantum localization and the rate of exploration of phase-space*, Phys. Rev. A **35**, 1360 (1987).

[37] D. Cohen, V. I. Yukalov, and K. Ziegler, *Hilbert-space localization in closed quantum systems*, Phys. Rev. A **93**, 042101 (2016).

[38] L. Kaplan and E. J. Heller, *Measuring scars of periodic orbits*, Phys. Rev. E **59**, 6609 (1999).

[39] L. Kaplan, *Scars in quantum chaotic wavefunctions*, Nonlinearity **12**, R1 (1999).

[40] E. M. Montroll and G. H. Weiss, *Random Walks on Lattices. II*, J. Math. Phys. **6**, 167 (1965).

Author Contributions:
CK, AV and DC contributed to all aspects of this work.

Competing interests:
The authors declare no competing financial interests.

Corresponding authors:
CK ⟨khripkov@post.bgu.ac.il⟩,
AV ⟨avardi@bgu.ac.il⟩,
DC ⟨dcohen@bgu.ac.il⟩.

Semiclassical theory of strong localization for quantum thermalization

(Supplementary)

Christine Khripkov[1], Amichay Vardi[1], Doron Cohen[2]

[1]Department of Chemistry, Ben-Gurion University of the Negev, Beer-Sheva 84105, Israel
[2]Department of Physics, Ben-Gurion University of the Negev, Beer-Sheva 84105, Israel

In this supplementary we first provide an expanded pedagogic narrative for the figures of the main manuscript. Next, we explain a few important details regarding the model system. Finally, we give a detailed description of the different types of simulation (classical, semiclassical and quantum).

Expanded description of the figures

Fig.1.– The unperturbed spectrum is schematically presented in Fig. 1b. From a semiclassical perspective, each unperturbed eigenstate represents a single cell in the classical phase-space, while each perturbed eigenstate represents an energy surface.

Fig.2.– Numerical results showing quantum localization are presented in Fig. 2. The system is launched in a single cell $r_0 = (x_0, \varepsilon_0)$ (quantum mechanically, in a single eigenstate of the unperturbed Hamiltonian $\mathcal{H}_0$). Evolving in time according to $\mathcal{H}$, transitions are induced by the coupling $\mathcal{H}_c$, leading to a time dependent probability $P_t(r|r_0)$ of finding the system at time t in each of the cells r, given it was initiated in the cell r_0. When the classical dynamics is chaotic, this distribution is expected to spread until it becomes uniform, and an equilibrium is reached. Panels 2a and 2b, show the long time saturation profiles of the distribution, $P_\infty(r|r_0)$, as obtained from semiclassical (propagation of an ensemble of classical trajectories) and full quantum calculations, respectively. The initial cell has all particles in the trimer subsystem, i.e., $x_0 = N$. This region of the (x, ε) space exhibits fully chaotic dynamics [2] and thermalization is therefore anticipated. While this expectation is fulfilled by the semiclassical distribution which has ergodically spread out, the corresponding quantum distribution remains localized around high x values.

All the initial conditions in our simulations lie on the same "horizontal" line $\varepsilon_0 = 1.181$. Thus, we omit ε_0 for simplicity, and identify each initial cell solely by its x_0. Correspondingly, we focus the discussion on the macroscopic trimer population x and extract the probability $P_t(x|x_0)$ of finding x trimer particles at time t, given the system was launched at x_0 (with implicit fixed initial energy ε_0). This is done by simply binning together all cells which have the same x, i.e., $P_t(x|x_0) = \sum_{r\in x} P_t(r|r_0)$ with $r_0 = (x_0, \varepsilon_0)$. The resulting semiclassical and quantum trimer-particle-number distributions at saturation are plotted in Panel 2c. The semiclassical distribution has approached its equilibrium limit which is in excellent agreement with the density of states $g(x)$ at the pertinent energy (the small deviations at low x_0 are explained by the semiclassical localization in this region, see below). However, the quantum distribution shows a clear localization of particles in the trimer subsystem. By comparison, if the system is launched in the range $30 \le x_0 \le 55$ thermalization is obtained both semiclassically and quantum mechanically (see Ref. [2]).

Panel 2d summarizes the results of propagation with various initial values of x_0 (e.g., in panels a–c the semiclassical and the quantum results correspond to the rightmost $\square$ and $\diamond$ symbols, respectively, in panel d). For each initial condition x_0 we plot the spreading width L_∞ of the saturation distribution $P_\infty(x|x_0)$ (see equation (S-4) in the Methods). Quantum localization despite fully chaotic dynamics is clearly evident at large initial trimer populations. Lower x_0 values give thermalization of both semiclassical and quantum distributions. Finally, at very low initial trimer population (near the lowest allowed value for the pertinent energy) localization is again observed for both classical and quantum distributions. This low-x localization is semiclassical in nature, i.e., it is attributed to integrable classical phase-space structures [2].

Fig.3.– The LDOS for three representative cells lying in the semiclassical-localization, ergodic, and quantum-localization regions, respectively, is shown in Fig. 3. In the ergodic case (panel 3b) the quantum LDOS fills the available classical energy shell volume, giving a high $\mathcal{F}^{\rm qm}$ values. By contrast, localization (panels 3a,c) is indicated by a partial filling, resulting in a low $\mathcal{F}^{\rm qm}$. We note that, contrary to the usual expectation, a small value of $\mathcal{F}^{\rm qm}$ arises not only when the quantum LDOS is sparse (as happens for low x_0, see Fig. 3a), but also when the quantum LDOS is much narrower than the classical envelope (happens for $x_0 \approx N$, see Fig. 3c). We also see that the LDOS-based ergodization measure $\mathcal{F}^{\rm qm}$ is correlated with the "spatial" localization of the perturbed eigenstates (i.e., within a narrow x range), as seen in the color-coding of Fig. 3d. Additionally, there is a correlation with the dynamical localization that is demonstrated in Fig. 2. The y-scale in panels a–c is actually the integrated LDOS $(2\pi/\Delta)\int \rho(E)\, dE/2\pi$, where $\Delta = 50\Delta_0$. This scaling significantly improves the resolution of the figure.

Fig.4.– The unperturbed eigenstates $|r\rangle = |x, \varepsilon\rangle$ are displayed in Fig. 4a. Each is color coded according to its value of $\mathcal{F}^{\rm qm}$. High values $\mathcal{F}^{\rm qm} \sim 1/3$ correspond to ergodizing states, whereas low values indicate localization. The low-energy and high-energy regions with low $\mathcal{F}^{\rm qm}$ lie outside the classically chaotic region, indicated in Fig. 1b. Similarly, localization on the low-x side of the wide central energy region is also attributed to integrability and proliferation of regular (quazi-periodic) structures in the classical phase-space (i.e., semiclassical localization). However, focusing on the high x part of the central energy region we see a zone of low $\mathcal{F}^{\rm qm}$ despite a very high chaoticity; this situation corresponds to many-body localization. To complete the picture, the exact eigenstates $|E_\alpha\rangle$ of the perturbed Hamiltonian $\mathcal{H}$ are displayed in Fig. 4b. The eigenstates are positioned according to $x = \langle \hat{x} \rangle_\alpha$ and $\varepsilon = \langle \mathcal{H}_0 \rangle_\alpha$, and color-coded according to their x-variance. The low variance near $\langle \hat{x} \rangle_\alpha \approx N$ is again a clear indication of these eigenstates being close to the trimer number states $|r\rangle = |x, \varepsilon\rangle$ of the unperturbed system.

Fig.5.– The different functions of phase-space exploration and spreading are compared in Fig. 5 for one of the strongly localized cells $x_0 = 55$. The quantum exploration, or the participation number $\mathcal{N}_t^{\rm qm}$, initially grows like t/t_E. The linear phase ends quickly, resulting in a low saturation value $\mathcal{N}_\infty \ll \mathcal{N}_E$, indicating that only a small fraction of energy states within the energy shell participate in the dynamics of the quantum wavepacket. We see an early breakdown of QCC, apparent in the almost-immediate departure of the quantum and semiclassical spreading volumes, $\Omega_t^{\rm qm}$ and $\Omega_t^{\rm sc}$. We also observe the expected difference between the volume explored by a classical trajectory ($\Omega_t^{\rm cl}$) and the volume occupied by the spreading cloud of trajectories ($\Omega_t^{\rm sc}$). The breaktime t^*, indicated by the arrow, is extracted from the time when the QCC condition of equation (1) breaks down, at the intersection of the classical exploration $\Omega_t^{\rm cl}$ and the (appropriately scaled) semiclassical approximation $\mathcal{N}_t^{\rm sc}$ to the quantum exploration $\mathcal{N}_t^{\rm qm}$.

Fig.6.– In Fig. 6 we summarize the analysis for all the allowed values of x_0 (along the line $\varepsilon_0 = 1.181$). In Fig. 6a we plot the classical ergodicity measure $\mathcal{F}^{\rm cl}$ (blue). For ergodic dynamics we would expect to get the same value for all x_0, since if a trajectory visits the entire energy surface equally, it should make no difference where it is started. Indeed, we see a uniform value for almost all initial cells. A perfect ergodicity ($\mathcal{F}^{\rm cl} = 1$) is not possible by definition, since every energy surface contains both chaotic and regular regions. For the low x_0 values a significant portion of the cell becomes occupied by regular structures, and hence a smaller part of the energy surface is explored, leading to a lower $\mathcal{F}^{\rm cl}$ (the points $x_0 = 24$ and $x_0 = 23$, where it is indicated by Fig. 2d that almost no spreading takes place, and hence any analysis is bound to fail, were removed from this figure.) We also plot the exploration-spreading ratio $\Omega_\infty^{\rm cl}/\Omega_\infty^{\rm sc}$ with its ergodic estimate based on equation (7) (black line). The good agreement despite imperfect ergodicity indicates that semiclassical clouds are *effectively* ergodic relative to the volume of the chaotic window in Fig. 1b (even though parts of each energy surface, where regular structures proliferate, remain unexplored).

In Fig. 6b we show the breaktime which was deduced from the classical simulation using equation (1). In Fig. 6c the quantum ergodization measure $\mathcal{F}^{\rm qm}$ (red, and its ergodic value, red line) is compared to the dynamical localization measure $\mathcal{F}^{\rm s}$ (blue, and its ergodic value, blue line). We again see that there are two types of localization in this model: For small x_0 the localization reflects a lack of ergodicity, while for large x_0, where chaos prevails, it is apparently of the Anderson, or many-body, type. The semiclassical estimate for the localization volume $\mathcal{F}_{\rm erg}^{\rm s} \Omega_{t*}^{\rm sc}$ (black) shows a great agreement with the true value $\Omega_\infty^{\rm qm}$ across a range of two orders of magnitude. Note that this semiclassical estimate involves only the results of the classical simulations without any quantum data or interference corrections. Thus, while many-body localization is not explicitly present in the classical simulations, it can nevertheless be inferred from them through the semiclassical determination of the quantum breaktime.

Arnold diffusion

An isolated M-site Bose-Hubbard system has $f = M - 1$ classical degrees of freedom. Its $2f$ coordinate phase-space is filled by $d_E = 2f - 1$ dimensional energy surfaces, and additionally contains many $d_T = f$ dimensional invariant surfaces, so-called KAM tori. One wonders whether these KAM tori can serve as separatrices that completely separate different regions of the energy surface, and block any motion between them. The answer is that this is not the case if $d_E > d_T + 1$, which implies $M > 3$. It follows that in our $M = 4$ site model a typical classical trajectory can move between the chaotic and the regular regions, and the motion tend to be globally ergodic. However, this process, called Arnold diffusion, might be extremely slow, and cannot be observed on realistic simulation times. For example, our results show that the semiclassical localization for $x_0 = 23$ persists beyond $t = 20,000$.

General remarks on the four-site model

Quantization of the classical phase-space

In our four-site N-particle model system, quantum dynamics proceeds within a Hilbert-space of dimension $\mathcal{D}_N \sim N^3$. By contrast, classical dynamics happens in a much smaller phase-space defined by the canonically conjugate variable pairs, for example, the population n_j and the phase φ_j for each site $j = 0, 1, 2, 3$. However, of the four populations only three are independent, because the total number of particles is constant. Additionally, in the classical limit the Hamiltonian equation (9) contains only the relative phases between pairs of different sites, and of these, again, merely three are independent. Hence the system has a six-coordinate $d = 3$ dimentional classical phase space.

To generate a correspondence between a unitary quantum evolution and a classical motion we must assign a phase-space cell r to each unperturbed state $|r\rangle$. The unperturbed spectrum is resolved on a grid $|x, \varepsilon_m\rangle$, where the index $m = 1, 2, \ldots$ counts the states within a given x band. Therefore, it is reasonable to define the cell r as the phase-space region bounded by the four surfaces $(x - 1, x; \varepsilon_n, \varepsilon_{n+1})$. Here we are motivated by the standard description of a chaotic eigenstate in terms of a microcanonical energy shell of thickness h^d. Applying the same idea to all $|r\rangle$ states regardless of their chaoticity, we conclude that the volume h^d of each cell is determined by the "Planck constant" $h = V/\mathcal{D}_N$, where V is the total phase-space volume.

The assymetry apparent in our definition becomes insignificant at the high values of N where a quantum-classical correspondence is expected. However, it should be noticed that these cells are improper, as the product of lengths along each pair of conjugate coordinates is not equal to h. To explain this statement, consider a generic $d = 2$ phase-space with four coordinates (q_x, p_x, q_y, p_y). A proper Planck cell is one which has equal lengths for all coordinate pairs, meaning $dq_x\, dp_x = h$ and $dq_y\, dp_y = h$, and therefore its volume is $(dq_x\, dp_x)(dq_y\, dp_y) = h^2 = h^d$. In an improper cell the total volume is correct, but the lengths are different; for example, $dq_x\, dp_x = (1/100)h$ and $dq_y\, dp_y = 100h$, but still $(dq_x\, dp_x)(dq_y\, dp_y) = h^2$. For our cells, since the energy ε is a complicated function of the conjugate pairs n_j and φ_j, it is highly unlikely that we would get the correct product $dn_j d\varphi_j = h$ for each cell. The only thing we know for certain is the total cell volume, h^d, since it is implicit in the definition.

Identifying chaotic phase space regions

Consider the unperturbed spectrum with its banded structure. The energies within each x band are identical to those of an isolated trimer containing x particles, plus a constant $U/2(N - x)^2$ contributed by the monomer. Since the classical trimer has two degrees of freedom (three contributed by the three sites, but one eliminated due to conservation of particles), but only one constant of motion (its energy), any nonlinearity present in the equations of motion will generate phase-space regions where the dynamics is chaotic. The nonlinearity of the trimer is quantified by the ratio Ux/K. Coming back to the unperturbed tetramer spectrum, for $x \approx 0$ the classical energy surfaces are regular because the nonlinearity is too small. At higher x values, the central parts of each band become chaotic, while both the upper and the lower parts remain regular. That is because at the highest trimer energies the coupling is negligible, and so the individual site populations become additional constants of motion, whereas at low energies it is the nonlinear interaction which becomes negligible.

To summarize, the unperturbed spectrum of the tetramer system should contain a chaotic window, whose exact size and shape is determined by both N and UN/K (the latter being the maximum value of the trimer nonlinearity Ux/K). For our choice of parameters, this window is shaped like a wide curved wedge (see Fig. 1b). According to the KAM theorem, under a weak perturbation most of the regular phase-space structures (KAM tori) survive, acquiring only small deformations. Therefore the unperturbed spectrum can accurately predict the energy range where the dynamics generated by the perturbed Hamiltonian is chaotic.

Numerics and analysis of the simulations

The energy shell

The geometry of the energy shell is characterized by the semiclassical kernel $\rho^{sc}(r|E)$ that measures the overlap between phase-space regions occupied by a cell r and by an energy surface E. Regarded as a function of E for a given $r = r_0$, it is known as the local density of states (LDOS). From the LDOS we can evaluate a constant $\mathcal{N}_E$ that quantifies the size of the energy shell by counting the number of energy surfaces E overlapping with the initial cell r_0. In a similar way, we define the constant Ω_E that counts the number of cells overlapping a typical energy surface E, which lies within the energy range where the LDOS is finite and significant. For a classically ergodic system, $\Omega_E = \Omega^{\rm cl}_\infty$ is the phase-space volume that is explored by a very long, ergodic trajectory. In such systems, the accessible volume of the energy shell (as measured by the infinite-time spreading volume $\Omega^{\rm sc}_\infty$) is expected to satisfy equation (7). Since each cell has a unique LDOS, $\mathcal{N}_E$ depends on r_0. By contrast, Ω_E is a generic value independent of r_0, since a trully ergodic trajectory simulated for an infinite time should yield the same value regardless of its starting location.

In practice, our system is not ergodic by definition due to the presence of KAM surfaces, and therefore Ω_E cannot be determined from $\Omega^{\rm cl}_\infty$ even for trajectories initiated within the chaotic window. However, we can employ the equipartition theorem that equates the equilibrium probability to occupy a phase-space region with the volume of that region. Thus for an ergodic trajectory moving on an energy surface E, the total probability to reside within a cell r should be proportional to the overlap $\rho^{sc}(r|E)$ between this cell and the energy surface.

Classical exploration

Consider a classical trajectory, initially (at $t = 0$) located within the phase-space region belonging to some cell r_0. As the dynamics is initiated, the trajectory will move within the boundaries of r_0, until at some later time t it would have crossed over to a different cell r. At yet later time the trajectory may either continue to a third cell r', or return back to r_0. Proceeding in this manner, and using short time steps dt, we can track its entire history and calculate the probability to visit a given cell up to time t. A function of this probability, the classical explored volume $\Omega^{\rm cl}_t$ counts the number of cells visited by the trajectory during time t.

It is important to distinguish between the exploration of phase-space, referring to the volume covered by a single classical trajectory, and a spreading in phase-space, referring to the combined exploration by a semiclassical cloud of trajectories. A clear distinction between the two is crucial because high-dimensional spreading is reflected in having $\Omega^{\rm cl}_t \ll \Omega^{\rm sc}_t$ during the time evolution. The two volumes become identical only in one dimension.

Quantum exploration

The notion of quantum exploration was introduced by Heller [36] in connection with the dynamics of the survival probability, and its definition bears a strong resemblence to the classical exploration function $\Omega^{\rm cl}_t$. We define $\mathcal{N}^{\rm qm}_t$ as the number of perturbed quantum states $|E\rangle$ that participate in the dynamics of an unperturbed state $|r_0\rangle$ up to time t. Thus, while the classical function $\Omega^{\rm cl}_t$ explores cells lying on an energy surface E, the quantum function $\mathcal{N}^{\rm qm}_t$ explores energy states contributing to the time-evolved wavepacket initiated in $|r_0\rangle$. The saturation value $\mathcal{N}_\infty \equiv \mathcal{N}^{\rm qm}_\infty$ can be derived directly from the quantum LDOS $\rho^{qm}(r_0|E) = |\langle r_0|E\rangle|^2$.

The different notations Ω and $\mathcal{N}$ for the classical and the quantum simulations emphasize that the former explores the r cell-space, while the latter explores the E state-space. When proper Planck cells are used, $\mathcal{N}^{\rm qm}_t$ and $\Omega^{\rm cl}_t$ should coincide for a very short time, namely up to the Eherenfest time ($\sim \ln(1/\hbar)$), and then depart.In the idealized picture of a strong chaos, the classical count of cells then climbs very quickly to the ergodic value Ω_E, while the quantum count of states behaves roughly linearly until it saturates at the Heisenberg time t_H (or, more correctly, at $\sim t_H/3$, see equation (1)) to the value $\mathcal{N}_\infty$.

Simulations

The quantum dynamics is generated by the unitary propagation $|\psi_t\rangle = \exp(-i\mathcal{H}t)\,|\psi_0\rangle$, where the initial state is $|\psi_0\rangle = |r_0\rangle$.

The classical simulation is supposed to arise from a single phase-space trajectory initiated within r_0. At the same time, it should be representative of the entire phase-space region belonging to r_0. To overcome this complication we perform a cell-averaging procedure. First, we select at random a set of $5,000$ points located within the boundaries of r_0. Second, by tracking the location of each trajectory at subsequent time instances $0, dt, 2dt \ldots$ we generate the classical distribution $P^{\rm cl}_t(r|r_0)$ that assigns a probability to visit a cell r during the time t. Next, for each trajectory we calculate Ω_t using equation (20). Finally, we average over the entire set of Ω to get the cell-typical exploration function $\Omega^{\rm cl}_t$.

The semiclassical simulation is generated by a cloud of $50,000$ trajectories, which are all initiated in random positions within the phase-space region belonging to cell r_0. Each trajectory is separately propagated by the Hamiltonian equations of motion. The combined positions of all the trajectories at time t form the probability distribution $P_t^{\rm sc}(r|r_0)$. Semiclassical functions such as $\Omega_t^{\rm sc}$ and $\rho(E)$ should by definition have a smooth dependence on their argument. Small fluctuations that may arise when the cloud size is insufficient can be removed by a local averaging (i.e., over a short time period for $\Omega_t^{\rm sc}$, or over a short energy range for $\rho(E)$).

When a cell contains large regions of quazi-periodic dynamics, a significant portion of the trajectories initiated in that cell lie on a KAM tori, and therefore during their history visit only a small number of cells. As a result, the exploration rate for such a cell will be significantly smaller than for one of the chaotic cells, and accordingly, the spreading rate will also become small.

For our analysis it is necessary to know the saturation values of the different time dependent functions. Due to computational limitations, a full saturation is not reachable: the weak perturbation induces slow exploration rates, which are further depressed by localization effects. As a compromise, we proceed the simulations up to the time when the growth rate of the various Ω functions becomes very slow, such that any cutoff tails are deemed to give a negligible contribution. In terms of actual numbers, we stop the quantum and the semiclassical simulations after $t = 10,000$ (except for $x_0 = 25$ and $x_0 = 26$, where the final times are $t = 25,000$ and $t = 20,000$, respectively), while the significantly slower classical simulation is stopped at $t = 20,000$.

Time averaging and the quantum saturation values

In general, due to its quantum nature, the dynamics of the spreading function $\Omega_t^{\rm qm}$ always displays fluctuations. For the nonlocalized states, which have a wide LDOS, those fluctuations are relatively weak, and a well-defined saturation value $\Omega_\infty^{\rm qm}$ can be derived by a local smoothing of $\Omega_t^{\rm qm}$, (i.e., by averaging over a short time period following a sufficiently long simulation time). However, for the nonlocalized states those fluctuations are much stronger, remaining significant even after extremely long simulation times, A logical solution is to *define* the saturation values as

$$\Omega_\infty^{\rm qm} \equiv \lim_{t\to\infty} \overline{\Omega_t^{\rm qm}} \tag{S-1}$$

where the bar above Ω indicates a time average. The same reasoning applies also in the case of the probability distribution $P_t^{\rm qm}(r|r_0)$. In fact, the saturation profile of equation (19) is exactly equal to the infinite-time average of $P_t^{\rm qm}(r|r_0)$. It is tempting to conclude that the value $\Omega_\infty^{\rm qm}$ can be found directly from the saturation profile through the application of equation (20). However, it is easy to see that this is not the case:

$$\lim_{t\to\infty} \overline{\Omega_t^{\rm qm}} = \lim_{t\to\infty} \frac{1}{t}\int_0^\tau \Omega_\tau^{\rm qm} d\tau = \lim_{t\to\infty} \frac{1}{t}\int_0^\tau d\tau \left\{\sum_r \left[P_\tau(r|r_0)\right]^2\right\}^{-1} \neq \left\{\sum_r \left[P_\infty(r|r_0)\right]^2\right\}^{-1} \tag{S-2}$$

For the sake of consistency, the infinite-time averaging must be applied for all quantum simulations, even those which do not localize. However, this creates no problems: by definition, a function that saturates retains forever the same value, and hence an averaging over a sufficiently long time yields back the saturation value.

One-dimensinal spreading in x

The two-dimensional distribution $P_t(r|r_0)$ gives the probability to move from cell r_0 to cell r after a time t. Contracting along the "vertical" energy axis we obtain the one-dimensional distribution $P_t(x|x_0)$. It describes the overall probability to move from the initial "horizontal" position x_0, with $r_0 = (x_0, \varepsilon_0)$, and some other position x.

$$P_t(x|x_0) = \sum_{r\in x} P_t(r|r_0) \tag{S-3}$$

The sum is performed over all cells $r = (x, \varepsilon)$ belongind to the same x band. In the spirit of equation (20) we define the spreading length in x,

$$L_t = \left\{\sum_x \left[P_t(x|x_0)\right]^2\right\}^{-1} \tag{S-4}$$

Its saturation value L_∞ determines the maximum range of x accessible to the dynamics, and thus the ratio $L_\infty^{\rm qm}/L_\infty^{\rm sc} < 1$ serves as an indicator of quantum localization in the x coordinate.